THE LHCb EXPERIMENT*

T. Nakada

On behalf of the LHCb Collaboration

CERN, Physics Department, Geneva, Switzerland
and
EPFL, Laboratory for High Energy Physics, Lausanne, Switzerland

(Received November 15, 2006)

LHCb is designed to search for physics beyond the Standard Model by studying CP violation and other rare processes in the B meson system with high precision at LHC. It has a flexible trigger system efficient for both leptonic and hadronic final states, particle identification capability over large momentum range and excellent decay time resolution. Construction and installation of various detector components are advancing well and the experiment is expected to be ready for the start-up of the LHC operation.

PACS numbers: 29.40.–n

1. Introduction

The current status of the quark flavour physics can be summarised as a tremendous success of the Cabibbo–Kobayashi–Maskawa prescription [1, 2] for the charged current weak interactions. The impressive number of results obtained by BABAR and BELLE experiments on B meson decays [3], as well as the recent measurement of the B_s^0–$\overline{B}_s^0$ oscillation frequency by the CDF experiment [4], can be illustrated by a plot on the ρ–η plane, where ρ and η are two of the four parameters of the Wolfenstein representation [5] of the Cabibbo–Kobayashi–Maskawa quark mass mixing matrix (CKM) [2]. Fig. 1 is an example from the CKM-fitter group [6]. It shows that all the measurements are clearly converging on a unique solution of $(\rho,\ \eta)$.

If one includes a possibility of physics beyond the Standard Model by allowing new particles contributing to the loop processes, all the box and penguin diagrams receive additional strengths and phases. A solution for $(\rho,\ \eta)$ obtained from $|V_{\rm ub}|^2 \propto \rho^2+\eta^2$ and $\gamma = \tan^{-1}\eta/\rho$, which are extracted

* Presented at the "Physics at LHC" Conference, Kraków, Poland, July 3–8, 2006.

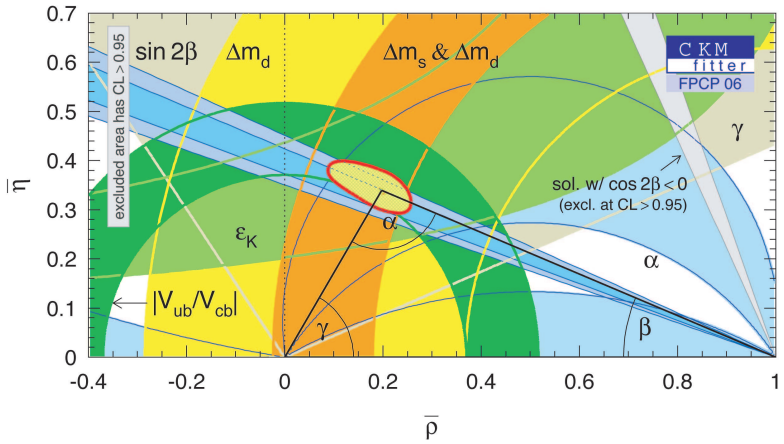

Fig. 1. Constraints on the Wolfenstein parameters ρ and η from various measurements.

from semileptonic B decays and $B \to DK$ decays respectively, gives the true CKM parameters unaffected by possible new physics. On the other hand, a solution obtained from $|V_{\rm td}|^2 \propto (1-\rho)^2+\eta^2$ and $\beta = \tan^{-1}\eta/(1-\rho)$, which are extracted from the processes involving B–$\overline{B}$ oscillations, can be a wrong one due to the contribution from new physics. In this case, the two solutions could disagree. For such a study, the current error on the measurement of the angle γ needs to be reduced by a factor of five or more in order to have the two solutions with comparable accuracy. Note that the accuracy on γ and β is dominated by the experimental errors, while theoretical errors dominate for $|V_{\rm ub}|^2$ and $|V_{\rm td}|^2$.

While the B–$\overline{B}$ oscillation phase with respect to $V_{\rm cb}$ is well measured for the $B_{\rm d}$ meson system with a relative accuracy of 5%, we need more than two orders of magnitude improvement to reach a sensitivity equal to the Standard Model expectation for the $B_{\rm s}$ meson system. Clearly there is a lot of room for a surprise. Similarly, a two orders of magnitude improvement is needed to reach the sensitivity for observing the $B_{\rm s} \to \mu^+\mu^-$ decay in the Standard Model.

Another interesting way to search for evidence of a new physics contribution is to look for a deviation from the V–A Lorentz structure of the electroweak current in the loop processes. This could be done by studying the angular distribution of $\mu^+\mu^-$ pairs in an appropriate coordinate system in the decay modes such as $B^0 \to K^{*0}\mu^+\mu^-$ and $B^0_{\rm s} \to \phi\mu^+\mu^-$. BABAR and BELLE statistics for the former mode would be still limited for reaching an interesting level of accuracy.

CP violation in $B^0 \to \pi\pi$, $\rho\pi$ and $\rho\rho$ is due to a mixture of box, tree and penguin diagrams. Therefore, an interesting prospect is present to study new physics there. Finally, the oscillation and CP violation in the D^0 meson system, expected to be very small in the Standard Model, could produce surprises.

The LHCb experiment will address those issues exploiting the large number of B^0, B_s and D^0 mesons produced at LHC, as well as $B^{\pm}$, B_c and b-baryons. The detector is optimised for heavy flavour physics having a trigger efficient for both leptonic and hadronic final states, an excellent decay time resolution to resolve the rapid B_s^0–$\overline{B}_s^0$ oscillation, an ability to distinguish kaons from pions essential for reconstructing the hadronic final states, as well as a good mass resolution mandatory for reducing the background. Contributions by Ivan Belyaev, Olivier Deschamps, Luis Fernandez, and Jonas Rademacker in these proceedings address the expected LHCb physics performance for specific physics issues. In this contribution, the status of the LHCb experiment is described.

2. The LHCb detector

Fig. 2 shows the layout of the LHCb detector [7]. The basic composition of the spectrometer remains unchanged from that of the Technical Proposal [8] produced in 1998. It consists of the dipole magnet, beam pipe, Vertex Locator, tracking system, two Ring Imaging Cherenkov detectors

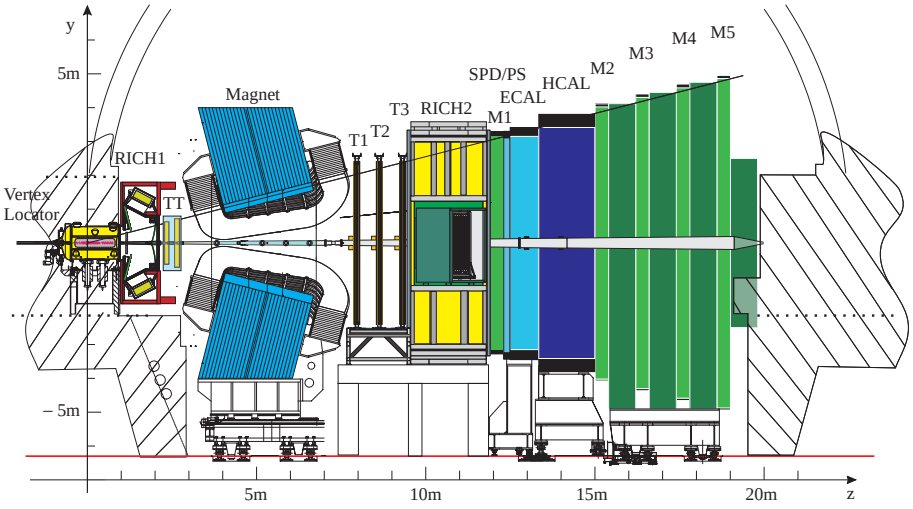

Fig. 2. Side view of the LHCb detector.

(RICH-1 and RICH-2) with three radiators, a calorimeter system and a muon system. Fig. 3 shows a recent photograph of the experimental area, where the magnet, tracking system support structure, RICH-2, calorimeter and muon systems are visible. Some more details are provided in the following sections.

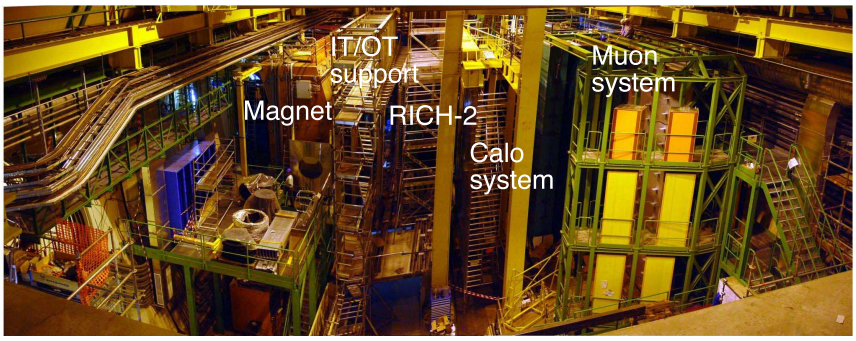

Fig. 3. A recent snapshot of the LHCb experimental area.

2.1. Dipole magnet

A large warm dipole magnet is used in the experiment [9]. The two coils are wound from hollow aluminium conductor; the shape of the coils follows the acceptance of the spectrometer. The magnet provides an integral field $\int Bdl = 4$ Tm and the power consumption is about 4.2 MW. The 1600 ton iron yoke and the coils have been assembled and placed in its final position as seen from Fig. 4. The magnet field has been mapped with all the iron structure of the experiment in place and it is ready to be used in data taking.

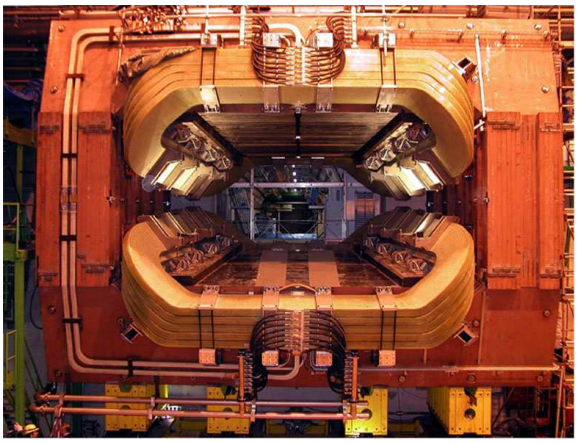

Fig. 4. The LHCb dipole magnet.

2.2. Beam pipe

A schematic view of the beam pipe is shown in Fig. 5. It comprises four major sections. The first section consists of a beryllium conical pipe with an opening angle of 25 mrad and a transition to the 10 mrad section. This beam pipe is welded to a spherical window of 2 mm thick aluminium that serves as the exit window of the vacuum vessel for the Vertex Locator. This section is followed by two further sections made of beryllium and a fourth section in stainless steel, all of conical shape with an opening angle of 10 mrad. The three beryllium sections are connected with aluminium flanges and bellows. Their positions are optimised to reduce background due to the production of secondary particles. Except for the third beryllium section, which is being tested now, the beam pipe is ready for installation.

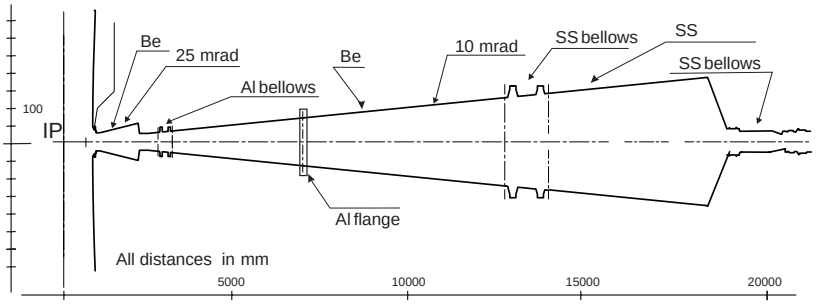

Fig. 5. Layout of the beam pipe.

2.3. Vertex locator

The Vertex Locator (VELO) consists of 21 pairs of silicon strip detectors arranged in two halves around the beam interaction region [7,10]. There are two types of sensors with different strip layouts, r-strips and ϕ-strips, with high spatial resolution. This strip geometry is designed for a fast track finding algorithm which is important as this detector is used in trigger. The primary vertex resolution is expected to be ~ 10 μm in the transverse plane and ~ 45 μm along the beam axis. The detector halves are located in a vacuum vessel, retractable and separated from the beam vacuum by specially formed aluminium foils of 0.3 mm thickness. The maximum allowable pressure difference across the foil is 10 mbar, therefore a complex vacuum control system is required. As seen from Fig. 6, the vacuum vessel has been constructed and installed at the collision point and its vacuum system is now being commissioned. Production of the sensor module is in progress.

Fig. 6. The VELO mechanics for holding the vacuum vessel.

2.4. Tracking system

The Tracking System consists of the Trigger Tracker (TT) [7], placed in between RICH 1 and the dipole magnet, and three tracking stations located downstream of the dipole in front of RICH-2. The three stations are subdivided into an Inner Tracker (IT) [11] located around the beam pipe and using silicon detectors and an Outer Tracker (OT) [12] using straw tube technology. A schematic layout is shown in Fig. 7.

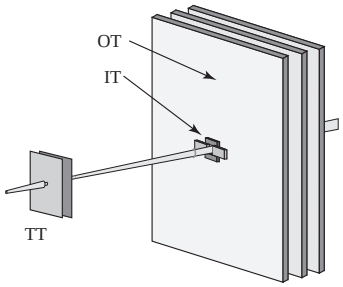

Fig. 7. Layout of the Tracking System.

Each station of the Outer Tracker consists of four planes of straw modules arranged with 0, +5, −5 and 0 degree with respect to the vertical axis. The 5 m long modules have double layers of straw tubes with 5 mm diameter; the 128 straws of each module are read out on both ends. All the modules have been constructed and their installation has started. Fig. 8 shows a

right-half of the second station where two layers of the modules are loaded on to the supporting frame. The supporting frame is already equipped with necessary cables and gas pipes.

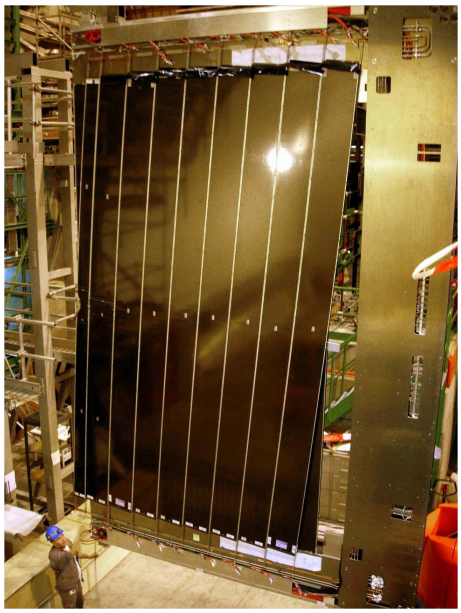

Fig. 8. Installed OT support frames with two layers of the detector modules.

The Trigger Tracker consists of four layers of silicon strip detectors each with an active area of about 1.4×1.2 m^2. The silicon sensors are 500 μm thick, 9.4 cm long and 9.6 cm wide, with a strip pitch of 183 μm. Seven sensors are put together and mounted on vertical ladders. The sensors are connected to the read-out electronics located outside the acceptance area by Kapton interconnect cables. Using the magnetic fringe field in front of TT, this detector is used in the early stage of the high level trigger to select events containing particles with high p_{T}. All the sensors have been delivered and tested, and as seen in Fig. 9 construction of the ladders is in progress.

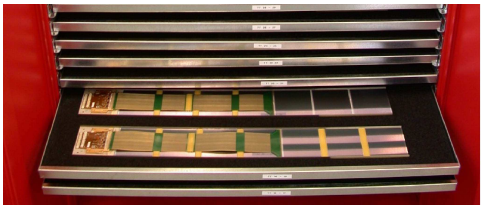

Fig. 9. Ladders of silicon wafers for the Trigger Tracker.

Fig. 10. Support frames for the Inner Tracker stations.

The three Inner Tracker stations are subdivided into four boxes of two types. One type of boxes are positioned at the top and bottom of the beam pipe and another type at the two sides. Silicon strip sensors with a thickness of 320 μm are used in the first type where they are arranged as one detector per column. For the second type, 410 μm thick sensors are used with two detectors per column. The sensors are 11 cm long and 7.8 cm wide with a strip pitch of 198 μm. Each box has four layers. All the sensors have been delivered and tested. Ladder production as well as the assembling of the support frames (shown in Fig. 10) is in progress.

2.5. Ring imaging Cherenkov counters

Particle identification in the range of 2–100 GeV/c is provided by two Ring Imaging Cherenkov (RICH) detectors [7,13]. RICH-1 is located directly behind the Vertex Locator and contains two radiators, aerogel and C_4F_{10}. In order to minimise material in the acceptance region, the detector is directly sealed to the vacuum vessel of the vertex locator and uses also the beam pipe as part of the gas enclosure. A set of spherical mirrors with a low-mass composite material (in the acceptance region) and planar glass mirrors

guide the photons towards two planes of photon detectors. Two massive magnetic shielding boxes protect the photon detectors from the stray field of the magnet and at the same time bring magnetic field into the region in front of the Trigger Tracker. The shielding boxes and the gas enclosure box have been installed and the stainless steel gas seal has been attached to the VELO vacuum tank, as seen from Fig. 11.

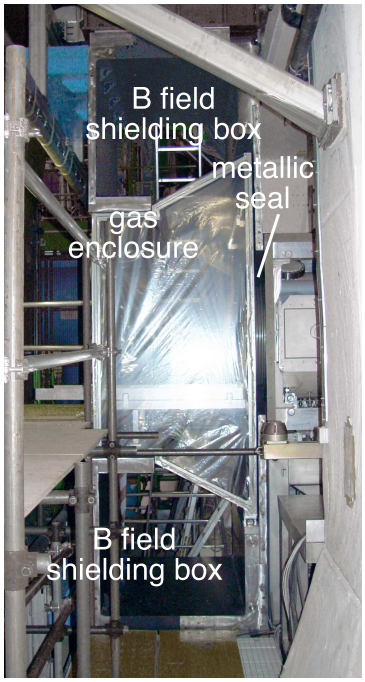

Fig. 11. RICH-1 magnetic shielding box, gas enclosure and gas seal to the VELO vacuum vessel installed in the final position.

The second RICH detector has a gas volume of 100 m^3 and uses CF_4 as radiator with a similar optical arrangement as RICH-1, however both spherical and planner mirrors are made of glass. The complete detector has been installed in the pit as shown in Fig. 12 waiting for the photon detectors.

Both RICH detectors will be equipped with so-called Hybrid Photon Detectors (HPDs) that have been developed in collaboration with industry. These photon detectors have a photocathode of 75 mm active diameter and incorporate a pixel silicon sensor bump-bonded to a binary read-out chip. The bump bonding of the pixel sensors has been completed and their encapsulation in the phototubes together with the photocathode is in progress.

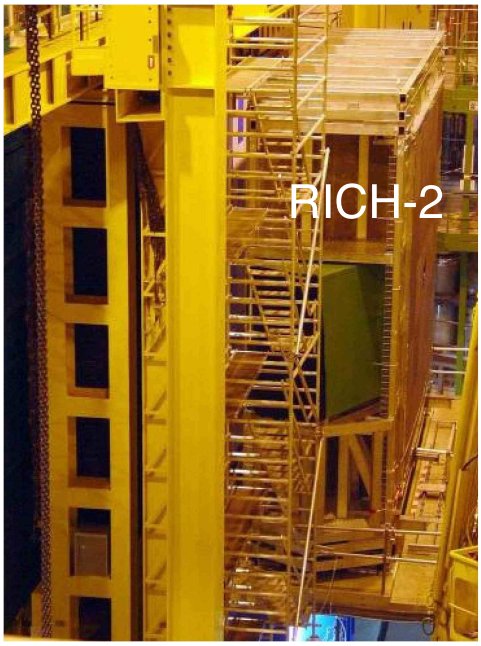

Fig. 12. The RICH-2 detector in the pit.

2.6. Calorimeter system

The calorimeter system [14] has three components: a combination of Scintillator Pad Detector and Pre-Shower Detector (SPD-PS), an Electromagnetic Calorimeter (ECAL) and a Hadron Calorimeter (HCAL). The SPD-PS consists of two layers of scintillator pads separated by a 1.5 cm thick lead wall. To adapt the granularity to the particle flux, there are three different sizes of scintillator pads. The light is collected by wavelength shifting fibres and guided to multi-anode photomultipliers located on the top and bottom of the detector. All the detectors and lead converter layer have been installed in the pit. The ECAL is of the Shashlik type and has a depth of 25 radiation lengths. It is divided into three regions with different cell sizes. All 3300 modules have been produced and assembled in the experimental area. The commissioning work has started.

The HCAL is an iron/scintillator calorimeter with tile geometry. It is also divided into three regions with different readout cell sizes. Production of the 52 modules has been finished and installed in the pit. The commissioning work has started.

2.7. Muon system

The muon detector consists of five stations [15]: one is located in front of the calorimeters and the four other stations behind are interleaved with an iron filter. The detector has a projective geometry, the stations are subdivided into four regions. The five detector planes will be equipped with 1380 multi-wire proportional chambers (MWPC), with the exception of the region of the highest rate at the centre of the first station that will be equipped with triple GEM chambers. Each station has four active gaps, where two are logically OR'd, except the first station that has only two layers to minimise material in front of the calorimeter. Depending on the track density, the readout is performed using the signals of the wires, the pads or both. They are connected to form logical pads and the total of about 26'000 channels is used in the Level-0 trigger. Close to 90% of the required MWPCs have been already produced. All the iron filter and the chamber mounting walls together with the balconies for gas and electronics racks have been installed. In parallel with the installation of cables and gas pipes on the walls, mounting of the chambers will start soon.

2.8. Trigger

An efficient and robust trigger is essential for this experiment. The original LHCb trigger system [16] was based on three layers: Level-0, Level-1 and High Level Trigger (HLT). The Level-0 trigger is unchanged and employs custom-made electronics using the information from the calorimeters, the muon detectors and the pile-up system to select events containing particles with high transverse momentum. The Level-0 trigger reduces the rate from 40 MHz to 1 MHz. In the original scheme, this rate is then further reduced to 40 kHz by the Level-1 trigger, a software algorithm running on a CPU farm and refining the event selection by adding the information from the Vertex Locator and the Trigger Tracker only, before reading out the entire detector information. With rapid progress in the networking technology, an affordable solution can be found already now which allows to readout the entire detector information and transfer them to a CPU farm at 1 MHz. This scheme gives a maximal flexibility and robustness in the trigger system. After HLT selection, data are stored at a rate of 2 kHz. The amount of stored data is ten times more than originally anticipated. The data now include a large amount of calibration data which are essential to understand systematics in the measurements. Details can be found in the contribution by Jose Angel Hernando-Morata in these proceedings. The electronics for the Level-0 trigger has been prototyped and production has started. Tests with the first version of the HLT software suite run on the prototype data acquisition system have validated the design of the system.

2.9. Computing

The data acquisition system is based on a large computing farm comprising some 1800 commodity processors [16, 17]. A commercial high performance Giga-bit Ethernet network switch is used to deliver the entire detector information to the CPU farm at a rate of 1 MHz. The complete system has been defined and the components needed at the start-up have been purchased. Fig. 13 shows the network switch.

Fig. 13. The network switch to be used in the LHCb data acquisition system.

An Experimental Control System based on the PVSS control framework is being built to control and monitor the LHCb experiment in a unified manner. The framework is developed as a joint research and development programme by the collaboration of four LHC experiments and CERN. All sub-detector groups have started to implement it for their system.

A complete chain of programs in C++ for the simulation, reconstruction and analysis has been put in place and is continuously being improved. A software framework for alignment and calibration is implemented and used by the sub-detector groups for their local alignment studies. A series of data challenges have successfully simulated and reconstructed a large number of events on distributed computing resources of the LHC Computing Grid. A framework for the distributed analysis is being tested.

3. Conclusions

The LHCb detector fulfils the requirements given by the physics goals. The quark flavour changing process in the Standard Model can be tested in a unique way using many reconstructed B mesons from the different final states, beyond the capabilities of current experiments at the e^+e^- B factories and the Tevatron. The construction of the detector is advancing well and the full physics programme is expected to start as soon as the LHC will become operational.

REFERENCES

[1] N. Cabibbo, *Phys. Rev. Lett.* **10**, 531 (1963).

[2] M. Kobayashi, T. Maskawa, *Prog. Theor. Phys.* **49**, 652 (1973).

[3] Some of the recent results from BABAR and BELLE experiments are summarised by Rainer Bartoldus for these proceedings.

[4] A. Abulencia *et al.* (CDF Collaboration), *Phys. Rev. Lett.* **97**, 062003 (2006).

[5] L. Wolfenstein, *Phys. Rev. Lett.* **51**, 1945 (1983).

[6] J. Charles *et al.* (CKMfitter Group), *Eur. Phys. J.* **C41**, (2005) 1, updated results and plots available at: http://ckmfitter.in2p3.fr

[7] R.A. Nobrega *et al.* (LHCb Collaboration), Reoptimized LHCb Detector Technical Design Report, CERN–LHCC/2003–30.

[8] S. Amato *et al.* (LHCb Collaboration), Technical Proposal, CERN-LHCC/98-4.

[9] S. Amato *et al.* (LHCb Collaboration), Magnet Technical Design Report, CERN–LHCC/2000–7.

[10] P.R. Barbosa Marinho *et al.* (LHCb Collaboration), Vertex Locator Technical Design Report, CERN–LHCC/2001–11.

[11] A. Franca Barbosa *et al.* (LHCb Collaboration), Inner Tracker Technical Design Report, CERN–LHCC/2002–29.

[12] P.R. Barbosa Marinho *et al.* (LHCb Collaboration), Outer Tracker Technical Design Report, CERN–LHCC/2001–24.

[13] S. Amato *et al.* (LHCb Collaboration), RICH Technical Design Report, CERN–LHCC/2000–37.

[14] S. Amato *et al.* (LHCb Collaboration), Calorimeter System Technical Design Report, CERN–LHCC/2000–36.

[15] P.R. Barbosa Marinho *et al.* (LHCb Collaboration), Muon System Technical Design Report, CERN–LHCC/2001–10;
LHCb Collaboration, Addendum to the Muon System Technical Design Report, CERN–LHCC/2003–2.

[16] R. Antunes Nobrega *et al.* (LHCb Collaboration), Trigger Technical Design Report, CERN–LHCC/2003–31.

[17] P.R. Barbosa Marinho *et al.* (LHCb Collaboration), Online System Technical Design Report, CERN–LHCC/2001–40.